City Research Online

City, University of London Institutional Repository

This is the accepted version of the paper.

This version of the publication may differ from the final published version.

Theoretical Analysis of a Non-Symmetric Polarization-Maintaining Single-Mode Fiber for Sensor Applications

Mohammad Karimi, F. Surre, Tong Sun, K. T. V. Grattan, W. Margulis, and P. Fonjallaz

Abstract—An asymmetric polarization-maintaining single-mode fiber with one side-hole being incorporated into the fiber cladding has been investigated analytically in this work for potential pressure measurements. The material birefringence of the fiber is calculated using a thermo-elastic displacement potential method through the superposition of sectional displacement potentials. The results obtained are generic and are thus applicable to any one-hole fiber structures, should the hole diameter or position vary in the fiber cladding, or the fiber hole be empty or filled in with any material. This enables the analysis to be applied more widely in a range of optical fiber sensor applications.

Index Terms—Displacement potential, fiber optic sensor, polarization-maintaining fiber, side-hole fiber, thermo-elastic.

I. INTRODUCTION

FIBER optic sensors have developed rapidly over the last three decades [1]–[3], incorporating novelty both in fiber structural design and in the sensing mechanisms used. They have shown advantages over conventional sensor technologies by being of small size, showing immunity to electromagnetic interference and resistance to chemical attack, for example, thus showing potential for both industrial and other practical measurement applications [4]. Among these, high-birefringence optical fibers have been widely explored for their potential for a variety of sensor applications, for example, for pressure measurements. High-birefringence optical fibers, such as fibers with an elliptical core or elliptical inner cladding, bow-tie, panda and photonic crystal fibers, have been widely investigated both numerically [5] and analytically [6], [7] and some of them have been made commercially available. All these fibers have shown symmetric structures in their designs.

This paper aims to explore the birefringence characteristics of fibers with non-symmetric structures by using a new analytical method to analyze one specialist polarization maintaining (PM) fiber containing one side-hole in the fiber cladding. To do so, a Poisson equation is used in this work to determine the stress
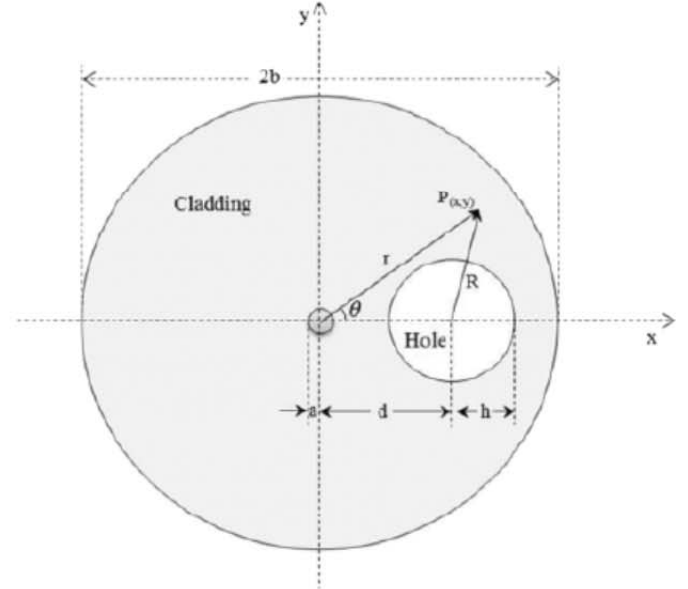
Fig. 1. One-hole PM fiber which has a core diameter $2a$ of 8.7 μm and hole diameter $2h$ of 30 μm. The distance between the right edge of the core to the left edge of the hole, $d - a - h$, is 9 μm.

distribution over the fiber cross-section by using cylindrical coordinates and a displacement potential formulation. The total stress in the fiber can thus be obtained with the superposition of the displacement potentials derived from each section of the fiber structure as the potential is a scalar.

II. ANALYTICAL METHOD

When the length of a fiber is sufficiently long (when compared to the fiber diameter) the calculation of stress in the fiber can be considered to be based on an infinite cylinder and therefore the 3-D strain measurements can be converted into 2-D measurements in polar coordinates either by superposing axial axis or by considering the axial strain to be zero if the external force is applied in a direction perpendicular to the fiber axis.

Fig. 1 shows schematically a PM fiber with one side-hole included in the fiber cladding. Thus the birefringence of the fiber, B, can be determined from [7]

$$B = C(\sigma_r - \sigma_\theta)\cos 2\theta - 2C\sigma_{r\theta}\sin 2\theta(\Delta\beta - \Delta\beta_0)l \quad (1)$$

where $C = 3.36 \times 10^{-5}$ mm^2/kg is the stress-optic coefficient of fiber, σ_r and σ_θ are stress components in polar coordinates,

respectively, and $\sigma_{r\theta}$ is a shear stress and these parameters can be given by [7]

$$\sigma_r = \frac{-E}{1+\nu}\frac{1}{r}\left[\frac{\partial\xi}{\partial r} + \frac{\partial^2\xi}{r\partial\theta^2}\right] \tag{2}$$

$$\sigma_\theta = \frac{-E}{1+\nu}\frac{\partial^2\xi}{\partial r^2} \tag{3}$$

$$\sigma_{r\theta} = \frac{E}{1+\nu}\frac{\partial}{\partial r}\left(\frac{\partial\xi}{r\partial\theta}\right) \tag{4}$$

again where $E = 7830$ kg/mm^2 and $\nu = 0.186$ are Young's modulus and Poisson's ratio, respectively. ξ is a sum of a total thermo-elastic displacement potential φ and Airy stress function A given by

$$\xi = \varphi + A. \tag{5}$$

The total thermo-elastic displacement potential φ is dependent on the fiber material and shape and is also related to the product $\propto T$ across the fiber cross-section expressed by the Poisson equation [8]

$$\nabla^2\varphi = \gamma_i T, \quad \gamma_i = \frac{1+\nu}{1-\nu}(\alpha_i - \alpha_2), \quad i = 1, 2, 3 \tag{6}$$

where index i refers to the region in the fiber, $i = 1$ refers to the fiber core and $i = 2$ and $i = 3$ refer to the fiber cladding and hole, respectively. ν is Poisson's ratio and α is thermal expansion coefficient and $T = 1650°$C is glass melting temperature.

Through the calculation of Poisson equation (6) for each section of the fiber, i.e., fiber core, cladding and hole, respectively; each sectional thermo-elastic displacement potential, φ_i, with i referring to the same sectional regions in the fiber as shown in (6), can thus be described as

$$\varphi_1(r) = \frac{\gamma_1 T}{4}r^2 + K_1 \quad \text{``inside core"} \quad r \leq a \tag{7}$$

$$\Phi_1(r) = \frac{\gamma_1 a^2 T}{2}\ln r + K_2 \quad \text{``outside core"} \quad r > a \tag{8}$$

$$\varphi_3(r) = \frac{\gamma_3 a^2}{4}R^2 + K_1' = \frac{\gamma_3 T}{4}(r^2 - 2rd\cos\theta + d^2) + K_1' \quad \text{``inside hole"} \quad R \leq h \tag{9}$$

$$\begin{aligned}\varphi_3(r) &= \frac{\gamma_3 h^2 T}{2}\ln R + K_2' \\ &= \frac{\gamma_3 h^2 T}{4}\ln(r^2 - 2rd\cos\theta + d^2) \\ &\quad + K_2' \quad \text{``outside hole"} \quad R > h \end{aligned} \tag{10}$$

where K_1, K_2, K_1' and K_2' are constant values and d is the distance between the centres of the fiber and of the hole and also φ_2 has a constant value.

In this work the Airy function is used to calculate the ξ as expressed in (5) and it is given by [7]

$$A(r,\theta) = b_0 r^2 + \sum_{n=1}^{\infty}\left(a_n r^n + b_n r^{n+2}\right)\cos(n\theta) \tag{11}$$

where Σ denotes summation over all of n ranging from 1 to ∞ and the coefficients a_n and b_n will be determined by using boundary conditions, which can be expressed as

$$\sigma_r = \sigma_{r\theta} = 0, \quad \text{when } r = b. \tag{12}$$

Based on the boundary conditions in (12) and taking into account of the superposed sectional thermo-elastic displacement potentials ($\varphi = \varphi_1 + \varphi_2 + \varphi_3$) illustrated in (8) and (10) and the Airy stress function A, ξ can be expressed as

$$\xi = \frac{\gamma_1 a^2 T}{2}\ln r - \frac{\gamma_3 h^2 T}{2}\left[\ln\frac{1}{r} + \sum_{n=1}^{\infty}\frac{1}{n}\left(\frac{d}{r}\right)^n\cos(n\theta)\right]. \tag{13}$$

In order to obtain the (13), a Green function is used

$$\begin{aligned}\ln\frac{1}{\sqrt{\rho^2 + \rho'^2 - 2\rho\rho'\cos(\omega - \omega')}} \\ = \ln\frac{1}{\rho_<} + \sum_{m=1}^{\infty}\frac{1}{m}\left(\frac{\rho_<}{\rho_>}\right)^m\cos[m(\omega - \omega')] \\ \rho_> = r, \rho_< = d. \end{aligned} \tag{14}$$

Then

$$\begin{aligned}\ln\left(r^2 - 2rd\cos\theta + d^2\right)^{-1/2} \\ = \ln\frac{1}{r} + \sum_{n=1}^{\infty}\frac{1}{n}\left(\frac{d}{r}\right)^n\cos(n\theta). \end{aligned} \tag{15}$$

Thus, the constant parameters shown in (11) can be given by

$$b_0 = -\frac{T}{4b^2}(a^2\gamma_1 + h^2\gamma_3) \tag{16}$$

$$a_n = \frac{\gamma_3 h^2 T}{2}\frac{(n+1)}{n}\left(\frac{d}{b^2}\right)^n \tag{17}$$

$$b_n = -\frac{\gamma_3 h^2 T}{2b^2}\left(\frac{d}{b^2}\right)^n. \tag{18}$$

As a result, all the stress equations can be derived by substituting (16), (17), and (18) into (11).

As illustrated in (5), the Airy stress function A and the total thermo-elastic displacement potential φ are independent parameters therefore their respective calculations can be done separately. This indicates that their associated fiber stress components can be calculated separately before being combined to form a total fiber stress. Following this, (2), (3) and (4) can be further expanded as follows for the Airy function:

$$\begin{aligned}\sigma_r^A &= \frac{ET}{1+\nu}\left\{\frac{a^2\gamma_1}{2b^2} + \frac{h^2\gamma_3}{2b^2} + \frac{h^2\gamma_3}{2}\right. \\ &\quad \times \sum_{n=1}^{\infty}\left[(n+1)(n-1)\left(\frac{d}{b^2}\right)^n r^{n-2}\right. \\ &\quad \left.\left. - (n+1)(n-2)\left(\frac{d}{b}\right)^n\frac{1}{b^2}r^n\right]\cos n\theta\right\} \end{aligned} \tag{19}$$

$$\sigma_\theta^A = \frac{ET}{1+v} \left\{ \frac{a^2\gamma_1}{2b^2} + \frac{h^2\gamma_3}{2b^2} - \frac{h^2\gamma_3}{2} \right.$$
$$\times \sum_{n=1}^{\infty} \left[(n+1)(n-1)\left(\frac{d}{b^2}\right)^n r^{n-2} \right.$$
$$\left. + (n+1)(n+2)\left(\frac{d}{b^2}\right)^n \frac{1}{b^2} r^n \right] \cos n\theta \right\} \quad (20)$$

$$\sigma_{r\theta}^A = -\frac{ET}{1+v} \left\{ \frac{h^2\gamma_3}{2} \left[\sum_{n=1}^{\infty} (n-1)(n+1)\left(\frac{d}{b^2}\right)^n r^{n-2} \right. \right.$$
$$\left. \left. - n(n+1)\left(\frac{d}{b^2}\right)^n \frac{r^n}{b^2} \right] \sin\theta \right\} \quad (21)$$

where superscript 'A' refers to Airy function.

Further, results obtained for inside the core are as follows:

$$\sigma_r^{core} = -\frac{ET}{2(1+v)}$$
$$\times \left\{ \gamma_1 + h^2\gamma_3 \frac{r^2 - d^2\cos 2\theta - 2rd\cos\theta}{(r^2 - 2rd\cos\theta + d^2)^2} \right\} \quad (22)$$

$$\sigma_\theta^{core} = -\frac{ET}{2(1+v)}$$
$$\times \left\{ \gamma_1 - h^2\gamma_3 \frac{r^2 + d^2\cos 2\theta - 2rd\cos\theta}{(r^2 - 2rd\cos\theta + d^2)^2} \right\} \quad (23)$$

$$\sigma_{r\theta}^{core} = \frac{ET}{1+v} h^2\gamma_3 d \frac{(r - d\cos\theta)\sin\theta}{(r^2 - 2rd\cos\theta + d^2)^2}. \quad (24)$$

And the results obtained for the cladding are

$$\sigma_r^{Cladding} = -\frac{ET}{2(1+v)}$$
$$\times \left\{ \frac{a^2\beta_1}{r^2} + \frac{r^2 - d^2\cos 2\theta - 2rd\cos\theta}{(r^2 - 2rd\cos\theta + d^2)^2} \right\} \quad (25)$$

$$\sigma_\theta^{Cladding} = -\frac{ET}{2(1+v)}$$
$$\times \left\{ -\frac{a^2\beta_1}{r^2} + \frac{r^2 + d^2\cos 2\theta - 2rd\cos\theta}{(r^2 - 2rd\cos\theta + d^2)^2} \right\} \quad (26)$$

$$\sigma_{r\theta}^{Cladding} = h^2\beta_3 d\sin\theta \frac{(r - d\cos\theta)}{(r^2 - 2rd\cos\theta + d^2)^2}. \quad (27)$$

The total stress of the fiber can be obtained by adding all the related stress components together, i.e., σ_r^A and σ_r^{Core} or $\sigma_r^{Cladding}$ for the core or the cladding, respectively.

As a result, (2)–(4) can be modified accordingly to be as follows:

$$\sigma_r = \sigma_r^A + \sigma_r^{Core/Cladding} \quad (28)$$
$$\sigma_\theta = \sigma_\theta^A + \sigma_\theta^{Core/Cladding} \quad (29)$$
$$\sigma_{r\theta} = \sigma_{r\theta}^A + \sigma_{r\theta}^{Core/Cladding}. \quad (30)$$

Finally, the fiber birefringence will be obtained by substitute (28), (29) and (30) into the (1).

The above detailed calculation has been aimed to determine the relationship between the birefringence of a one-hole fiber and several key parameters of the fiber structure, including the
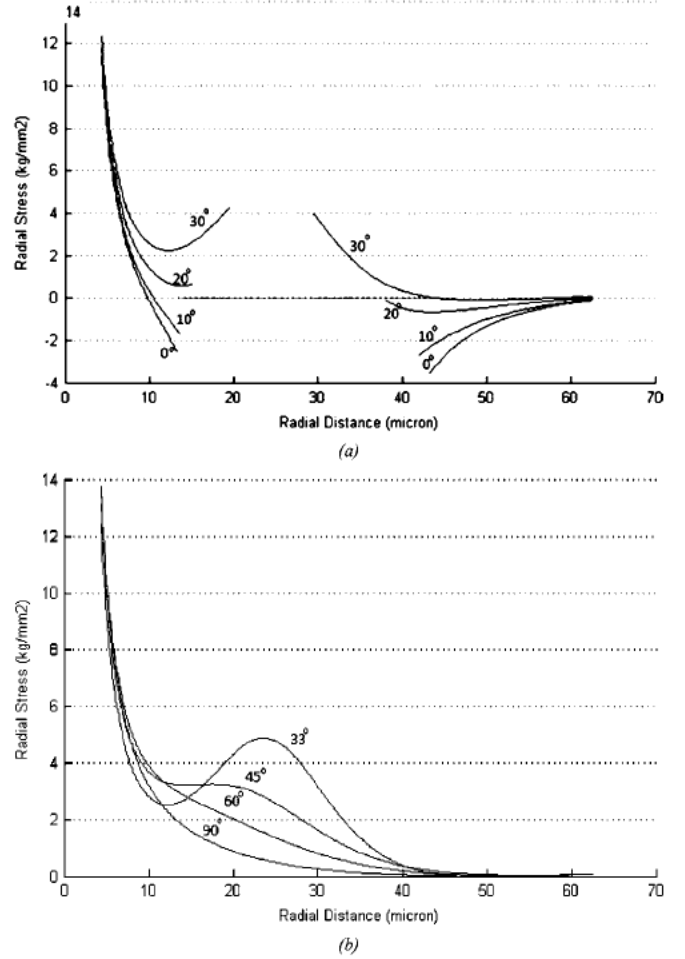

(a)

(b)

Fig. 2. Radial stress distribution in one-hole fiber as a function of radial distance r. (a) Radial stress distribution within the fiber cross-section with a hole, i.e., when θ varies from $0°$ to $30°$. (b) Radial stress distribution within the fiber cross-section outside the hole region when θ varies from $30°$ to $90°$.

size of the hole, the fiber materials, the hole position and the filling material inside the hole.

III. VALIDATION FOR SPECIALLY FABRICATED FIBER DESIGN

The fiber design shown in Fig. 1 was specially chosen for this case study as it has been successfully fabricated by colleagues at ACREO, Sweden. The fiber has a hole diameter ($2h$) of 30 μm and the distance between the right edge of the core to the left edge of the hole, $d - a - h$, is 9 μm. The fiber core diameter ($2a$) is 8.7 μm and clad diameter ($2b$) is 125 μm, $\alpha_1 = 2.125 \times 10^{-6} °C^{-1}$ and $\alpha_3 = 5.4 \times 10^{-7} °C^{-1}$ are core and cladding thermal expansion coefficients, respectively. The hole in the fiber is empty, i.e., there is no specific material being filled in.

Equations (28) and (29) are used to calculate the variation of radial stress (σ_r) and circumferential stress (σ_θ), respectively, as a function of r with different angle θ and the simulation results obtained are shown in Figs. 2 and 3. Fig. 2(a) illustrates the stress distribution in a fiber section where the hole is included, i.e., when θ varies from $0°$ to $30°$ and Fig. 2(b) shows the stress condition outside the hole region. Under both circumstances, it
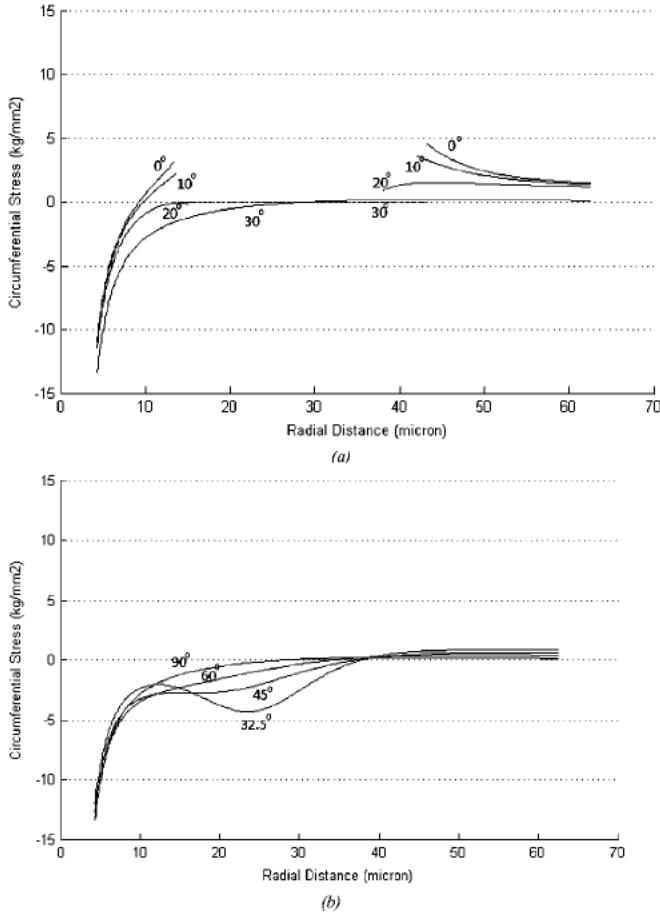
(a)

(b)

Fig. 3. Circumferential stress distribution in a one-hole fiber as a function of radial distance. (a) Circumferential stress distribution within the fiber cross-section with a hole, i.e., when θ varies from $0°$ to $30°$. (b) Circumferential stress distribution within the fiber cross-section outside the hole region when θ varies from $30°$ to $90°$.

Fig. 4. Stress distribution across the cladding.

(a)

(b)

Fig. 5. Birefringence distribution in a one-hole fiber core as a function of angles θ. (a) Edge of the core. (b) Cross of the core

is noticed that the radial stress varies with the increase of r but reach smoothly to zero as the radial distance moves towards the fiber boundary.

In Fig. 2(a), the radial stress has shown to decrease with the increase of r until when r is approaching the cladding boundary with the hole where a minimum stress has been observed. The stress profile inside the hole region in Fig. 2(a) is not shown as, under the simulation conditions, there is no material filling and therefore the stress is zero. At the cladding/hole boundary, some negative stress has shown to indicate the region is under compression. In Fig. 2(b), the radial stress has shown the decrease with the increase of r apart from the region which are affected by the existence of the hole when r scans from $\theta = 30°$ to $\theta = 45°$. Fig. 3 shows the circumferential stress, respectively, as a function of r with different angles, θ. It is noticeable that all the circumferential stress inside the fiber has been demonstrated to be negative, indicating the compression condition of the fiber. Again in Fig. 3(a) it has demonstrated a discontinuous profile due to the existence of the hole and the circumferential stress inside the hole is zero. In Fig. 3(b) a decrease of the compression has been observed with the increase of r apart from the region affected by the hole when r scans from $\theta = 30°$ to
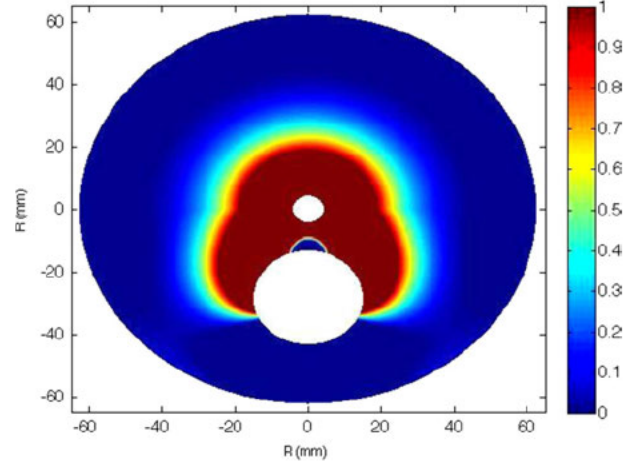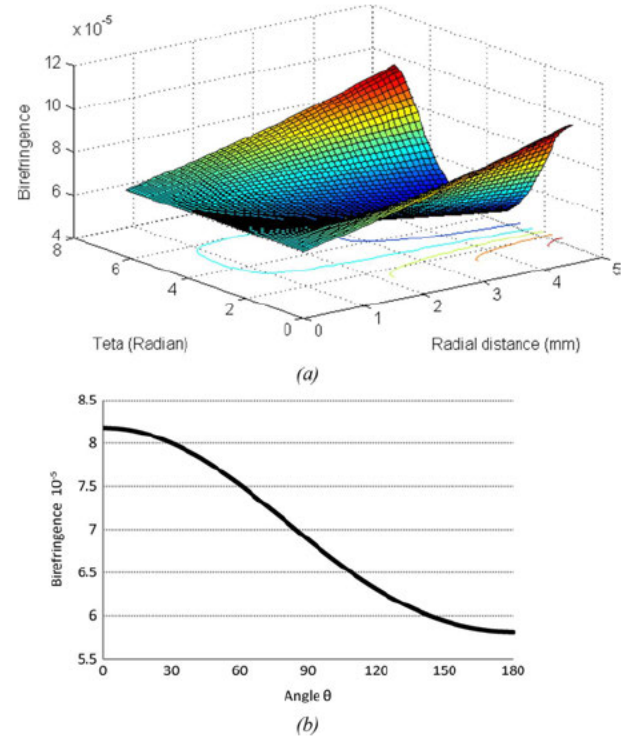
$\theta = 45°$. As shown in Fig. 3(b), in the region where there is no hole, a zero stress can be eventually reached at the edge of the fiber cladding, Fig. 4 shows a contour graph indicating the stress distribution across the fiber cladding. It is noticeable that the existence of the hole has changed the stress distribution profile within the fiber cladding. The stress is shown to be negative in some parts (dark blue) and positive (light blue) in others, with the maximum stress being near the fiber core.

In this graph stress inside the core (small white hole) and the hole (large white hole) is not considered.

Based upon the above, the fiber birefringence, as shown in (1), can be obtained. Fig. 5(a) and (b) show an expanded view of the birefringence in different directions. The stress-induced
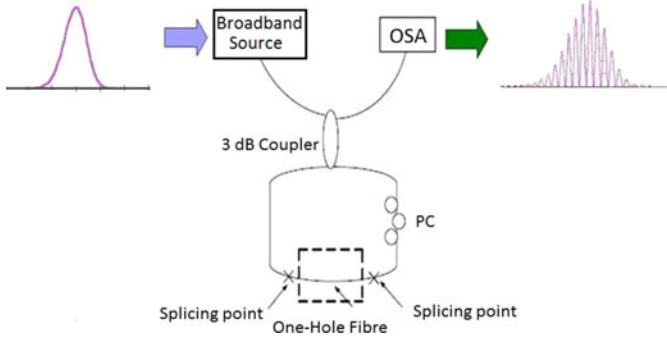
Fig. 6. Schematic setup of Sagnac loop interferometer incorporating the special birefringence fiber.
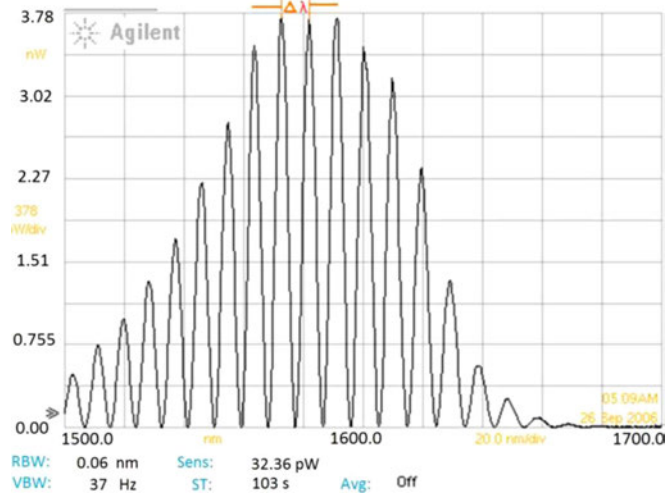

Fig. 7. Interference pattern from the Sagnac loop interferometer.

material birefringence of the fiber core shows birefringence at $\theta = 0$ is maximum (8.2×10^{-5}) then birefringence sinusoidal decrease until it reach to a minimum at $\theta = 180$.

IV. Experiments

In order to verify the above theoretical analysis, an experimental system, showing the potential for sensor applications, is set up and illustrated in Fig. 6.

As shown in Fig. 6, a 320 cm length of a PM fiber and a polarisation controller were fusion spliced between the two output ports of a directional optical coupler to form a Sagnac loop interferometer. One end of the interferometer is coupled to an optical broadband CW light source (with maximum output power of 3.42 mW and a central wavelength of 1550 nm with 55 nm bandwidth). The other end of the interferometer is connected to an optical spectrum analyzer, where the interferometer pattern, as shown in Fig. 7, can be seen.

As indicated in Fig. 7, the wavelength spacing between the peaks $(\Delta\lambda)$ is 9.26 nm. Generally the birefringence is inversely proportional to the wavelength separation between two output transmission peaks of a Sagnac interferometer [9]–[11] as illustrated in (31)

$$B = \frac{\lambda^2}{L\Delta\lambda}. \tag{31}$$

Therefore, the Birefringence of the fiber can be calculated to be 8.0×10^{-5} and this is very close to the theoretical results shown in Fig. 5. This result, however, has shown lower birefringence by comparison to that of most commercial fibers, such as panda fibers, to be approximately 4×10^{-4}. But this fiber is more sensitive to directional force compared to other symmetrical fibers such as panda and bow-tie fibers.

In summary, the above theoretical and experimental data have further confirmed the potential of this specialist fiber to be used as a sensor, for directional force measurements, which has been published elsewhere [12]

V. Discussions and Results

This paper has demonstrated successfully the use of a generic analytical method to calculate the birefringence and stress profile for non-symmetric fibers. This has been achieved through the superposition of sectional thermo-elastic displacement potentials coupled with the calculation of the Airy stress function.

This method is generic and thus can be used for any fiber birefringence analysis with or without the hole being filled with materials. The simulation results obtained have shown both a stress distribution inside the asymmetrical fiber as well as birefringence in the fiber core. In most cases non-symmetric fibers may demonstrate similar characteristics to symmetrical fibers when there is no external perturbation, but when non-symmetric fibers are used as sensors, they tend to demonstrate higher sensitivity to external changes, therefore it is important to have an optimized design of the fiber structure to enable a better sensor performance and this can be achieved by using the above method.

References

[1] K. T. V. Grattan and B. T. Meggitt, *Optical Fiber Sensor Technology*. Norwell, MA: Kluwer, 2000.

[2] Y. Shizhuo, P. B. Ruffin, and T. S. Yu Francis, *Fiber Optic Sensor*. New York: Taylor & Francis, 2008.

[3] B. Lee, "Review of the present status of optical fiber sensors," *Opt. Fiber Technol.*, vol. 9, pp. 57–79, 2003.

[4] T. R. Wolinski and A. W. Domanski, "Polarimetric optical fiber sensors of a new generation for industrial applications," *Bulletin Polish Acad. Sci. Tech. Sci.* , vol. 56, no. 2, pp. 125–132, 2008.

[5] A. N. Trufanov, O. Y. Smetannikov, and N. A. Trufanov, "Numerical analysis of residual stresses in preform of stress applying part for PANDA-type polarization maintaining optical fibers," *Opt. Fiber Technol.*, pp. 156–161, Jun. 2010.

[6] R. Guan, F. Zhu, Z. Gan, and D. Huang, "Stress birefringence analysis of polarization maintaining optical fibers," *Opt. Fiber Technol.*, vol. 11, pp. 240–254, 2005.

[7] Chu and Sammut, "Analytical method for calculation of stresses and material birefringence in polarization-maintaining optical fiber," *J. Lightw. Technol.*, vol. LT. 2, no. 5, 1984.

[8] S. P. Timoshenko and J. N. Goodier, *Theory of Elasticity*. Hoboken, NJ: McGraw-Hill, 1970.

[9] D. H. Kim and J. U. Kang, "Sagnac loop interferometer based on polarization maintaining photonic crystal fiber with reduced temperature sensitivity," *Opt. Exp.*, vol. 12, pp. 4490–4495, 2004.

[10] B. H. Kim, S. H. Lee, A. Lin, C.-L. Lee, J. Lee, and W.-T. Han, "Large temperature sensitivity of Sagnac loop interferometer based on the birefringent holey fiber filled with metal indium," *Opt. Exp.*, vol. 17, pp. 1789–1794, 2009.

[11] T. Xu, W. Jing, H. Zhang, K. Liu, D. Jia, and Y. Zhang, "Influence of birefringence dispersion on a distributed stress sensor using birefringent optical fiber," *Opt. Fiber Technol.*, vol. 15, no. 1, pp. 83–89, Jan. 2009.

[12] M. Karimi, F. Surre, T. Sun, and K. Grattan, "Directional force measurement using specialist single mode fibers," *J. Lightw. Technol.*, vol. 29, no. 24, pp. pp. 3611–3615, 2011.

Mohammad Karimi (M'11) received the B.Sc. degree in 1984 from Urrmia University, Urmia, Iran, the M.Sc. degree in physics from IUST, 2000, and the Ph.D. degree from the School of Engineering and Mathematical Sciences, City University London, London, U.K., in 2009.

His research involved the use of holography techniques interferometry for measurements on material expansion at IUST in the Optical Research Centre, London, U.K. From 2000 to 2001, he was a Researcher and Lecturer in Physics at Azad University, Tehran, Iran. His research interests include the diffusion in nanotube from 2002 to 2009.

Dr. Karimi is a Member of the Institute of Physics (IOP) and the International Society of Optics and Photonics (SPIE).

F. Surre received the Dipl. Eng., M.Sc., and Ph.D. degrees in electronic engineering from INPT-ENSEEIHT, Toulouse, France, in 1998, 1998, and 2003, respectively.

In 1998, he was a Research Engineer with Ecole Nationale de la Statistique et de l'Administration Economique (ENSAE), Toulouse, France, where he was responsible for opto/microwave measurements. In 2004, he joined the School of Physics, Trinity College, Hartford , CT, and RINCE, Dublin City University, Dublin, Ireland. His research interests include photonic devices for all-optical communications and generation and guiding of Terahertz waves. In 2008, he joined City University, London, U.K., to work on optical and terahertz sensors for structural health monitoring. He is chair of the IEEE Instrumentation and Measurement Technical Committee 16. He was chair of the topic Advances in Terahertz Devices and Applications in IEEE Photonics Winter Topicals Meeting 2010. He chaired the IEEE Student branch at ENSEEIHT in 2000 and he is currently Academic Advisor to the IEEE Student Chapter in Photonics at City University.

Tong Sun received the B.Eng. degree, M.S. degree in engineering, and the Ph.D. degree in engineering for work in mechanical engineering from the Department of Precision Instrumentation, Harbin Institute of Technology, Harbin, China, in 1990, 1993 and 1998, respectively. She also received the Ph.D. degree in philosophy from City University, London, U.K., in applied physics in 1999.

She was an Assistant Professor at Nanyang Technological University, Singapore, from 2000 to 2001 before she rejoined City University London, U.K., in 2001 as a Lecturer. Subsequently, she was promoted to a Senior Lecturer in 2003, a Reader in 2006, and a Professor in 2008 at City University. She has been leading a research team focused on developing a range of optical fiber sensors for a variety of industrial applications, including structural health monitoring, early fire detection, homeland security, process monitoring, food quality and automotive emission monitoring and has been working closely with partners across disciplines from academia and industry, both in the U.K. and overseas. She has authored or coauthored 130 scientific and technical papers.

Prof. Sun is a member of the Institute of Physics and of the Institution of Engineering and Technology and a Chartered Physicist and a Chartered Engineer, U.K.

K. T. V. Grattan received the B.Sc. (Hons.) in physics and the Ph.D. degree in laser physics from the Department of Physics, Queen's University, Belfast, U.K, in 1974 and 1978, respectively, and the D.Sc. degree from City University, London, U.K., in 1992 for his sensor work.

His research involved the use of laser-probe techniques for measurements on potential new laser systems. Following Queen's, in 1978 he became a Research Fellow at Imperial College of Science and Technology, London, U.K., sponsored by the Rutherford Laboratory to work on advanced photolytic drivers for novel laser systems. This involved detailed measurements of the characteristics and properties of novel laser species and a range of materials involved in systems calibration. In 1983 he joined City University, London, U.K. as a Lecturer in Physics, and was appointed Professor of Measurement and Instrumentation in 1991 and Head of the Department of Electrical, Electronic and Information Engineering. The work has been sponsored by a number of organizations including EPSRC, the EU, DERA, private industry and BTG, with whom a joint patent for systems for monitoring in the water industry is held. He has authored or coauthored of over 500 publications in major international journals and at conferences and is the co-editor (with Prof. B. T. Meggitt) of a five volume topical series on Optical Fiber Sensor Technology. His research interests include the use of fiber optic and optical systems in the measurement of a range of physical and chemical parameters.

Prof. Gratton is extensively involved with the work of the professional bodies, having been Chairman of the Science, Education and Technology of the Institution of Electrical Engineers, the Applied Optics Division of the Institute of Physics, and was President of the Institute of Measurement and Control in 2000. He has been Deputy Editor of the *Journal Measurement Science and Technology* for several years and currently serves on the editorial board of several major journals in his field in the U.S. and Europe. In January 2001, he was appointed Editor of the *IMEKO Journal Measurement* and also serves on their General Council. He is also Dean of the School of Informatics. He was also awarded the Callendar Medal of the Institute of Measurement and Control in 1992, and the Honeywell Prize for work published in the Institute's journal.

W. Margulis, biography not available at time of publication.

P. Fonjallaz, biography not available at time of publication.